

Optical modes in oxide-apertured micropillar cavities

Cristian Bonato,¹ Jan Gudat,¹ Keesjan de Vries,¹ Dapeng Ding,¹ Hyochul Kim,² Susanna M. Thon,³ Pierre M. Petroff,⁴ Martin P. van Exter,¹ and Dirk Bouwmeester^{1,4}

¹*Huygens Laboratory, Leiden University, P.O. Box 9504, 2300 RA Leiden, the Netherlands*

²*IREAP, University of Maryland, College Park, Maryland, USA*

³*Department of Electrical and Computer Engineering, University of Toronto, 10 King's College Road, Toronto, Ontario M5S 3G4, Canada*

⁴*University of California Santa Barbara, Santa Barbara, California, USA*

We present a detailed experimental characterization of the spectral and spatial structure of the confined optical modes for oxide-apertured micropillar cavities, showing good-quality Hermite-Gaussian profiles, easily mode-matched to external fields. We further derive a relation between the frequency splitting of the transverse modes and the expected Purcell factor. Finally, we describe a technique to retrieve the profile of the confining refractive index distribution from the spatial profiles of the modes.

Microcavities embedding single self-assembled quantum dots (QDs) are promising devices for the implementation of single photon sources[1] and hybrid quantum information applications based on cavity quantum electrodynamics[2]. For such applications, a large Purcell factor ($P = \frac{3}{4\pi^2} \left(\frac{\lambda}{n}\right)^3 \frac{Q}{V}$), is beneficial, i.e. the effective optical mode volume should be kept as small as possible, while maintaining a high quality factor Q . Moreover, it is crucial for the cavity modes to be easily mode-matched to an external field, either for efficient light collection or to get high-contrast dipole-induced reflection[2–4]. Finally, in applications involving the spin of a single electron in a dot, the integration of electrical contacts is crucial to have deterministic charge-tuning of the quantum dot.

Etched micropillars with quality factors exceeding 150000 have been demonstrated[5, 6]. Even though they do not allow for the smallest possible mode volume, because the cavity optical field extends into the Bragg mirror structure, they have been shown to reach the strong coupling regime[7]. The integration of electrical contacts in these structures, though possible, is not straightforward [8].

In oxide-apertured micropillars, the transverse optical confinement is determined by the difference in the effective refractive index between the oxidized and un-oxidized regions [9–11]. This creates a gentle confinement and significantly reduces the scattering compared to the rough side walls of etched micropillars. Moreover, structural contact to the bulk wafer is maintained, giving the ability to integrate electrical contacts in a convenient way [1, 4]. This enables controlled electron charging of the QD and fine-tuning of the optical transition frequency via the quantum-confined Stark effect. Finally, for application involving electron spins polarization-degeneracy of the cavity modes is required. This can be achieved for oxide-apertured micropillars in a non-invasive way, controlling strain by laser-induced surface defects burned far-away from the cavity region (which would not be possible for etched micropillars). [12, 13]

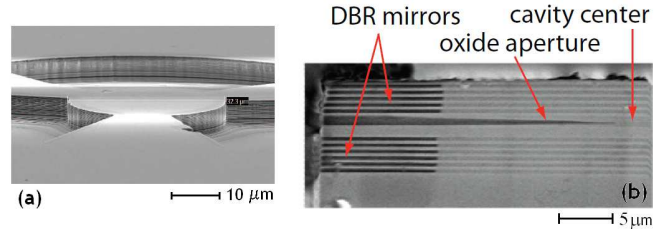


FIG. 1. (a) SEM view of a micropillar cavity with three trenches. (b) SEM cross section image of a typical micropillar with fewer DBR mirrors as used in the experiment. The oxide aperture in the middle has a linear profile in particular towards the center of the cavity where it stops before reaching the center and forms a very sharp edge.

In this paper, we present a detailed experimental characterization of the spectral and spatial profiles of the optical modes for oxide-apertured micropillar cavities, showing that these structures exhibit high-quality Hermite-Gaussian modes, easy to mode-match to external optical fields. Moreover, we introduced a technique to reconstruct the profile of the confining oxide refractive index profile from the experimentally measured mode profiles.

Micropillars are grown by molecular beam epitaxy on a GaAs [100] substrate. Two distributed Bragg reflector (DBR) mirrors consisting of alternating $\lambda/4$ -thick layers of GaAs and $\text{Al}_{0.9}\text{Ga}_{0.1}\text{As}$ (32 pairs for the bottom DBR and 23 pairs for the top DBR) embed the aperture layer and the active layer with InGaAs/GaAs self-assembled QDs. Trenches are etched down to the bottom DBR, leaving a circular pillar with a diameter of about 30 μm. The sample is steam-oxidized at 420°C (for a predetermined time based on calibration samples) to create an AlO_x oxidation front in the AlAs layer, leaving a small un-oxidized area in the center, with a diameter of 3–5 μm.

The optical modes are investigated by pumping the structure non-resonantly (785 nm, above the GaAs bandgap) with a few mW laser power. The pump beam,

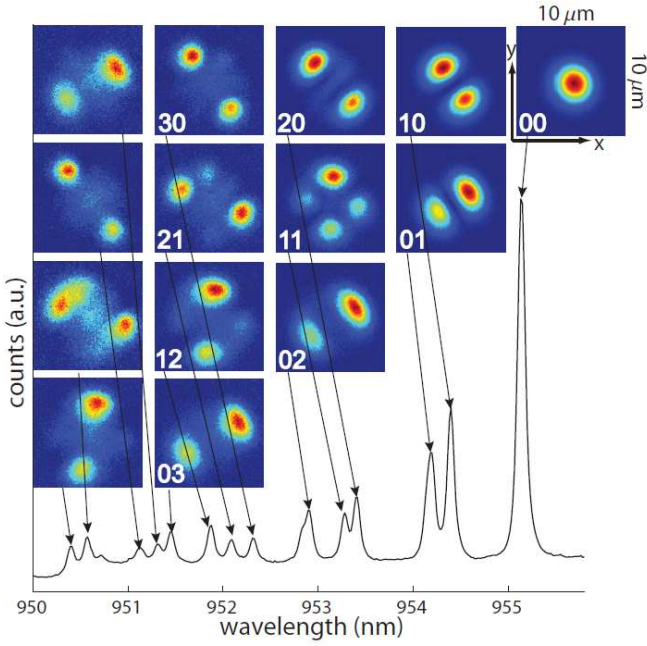


FIG. 2. Measured optical modes and spectrum of a non-polarization resolved spatial scan.

launched by a single-mode fiber collimated by a 20x microscope objective, is tightly focused on the sample by a microscope objective (100x, NA = 0.8) to a spot of about 1 μm . The photoluminescence is collected with a multi-mode fiber and spectrally resolved with a spectrometer (resolution 0.016 nm/pixel). In order to have a spatially-resolved photoluminescence plot, the excitation beam is scanned utilizing a piezo-driven xy-stage at a step size of 0.1 μm over an area of 10 \times 10 μm . Such a setup, spatially scanning the pump beam and collecting the emitted photoluminescence with no spatial-selectivity, allows us to probe the mode intensities within the cavity layer (under the assumption of a spatially-constant distribution of emitters). In other works, we are not imaging the far-field profiles of the cavity modes, but probing the optical near-field intensity within the cavity active region.

A non-polarization resolved measurement is presented in Fig.2. Two-dimensional spatial images are shown for the peaks of the spectrum. The spatial scans of the first ten peaks show clear features of Hermite-Gaussian modes and allow mode identification. The fundamental cavity mode fits to a Gaussian profile with high accuracy (99.94 \pm 0.06% in x - and 99.93 \pm 0.07% in the y -direction), allowing easy mode-matching to external fields.

In order to describe the optical modes we use an effective-index approximation[14], which simplifies the model by separating the longitudinal and transverse propagation and eliminating the longitudinal dependence by averaging it to an effective transverse confinement. We model the oxidation taper as a quadratic refractive in-

dex profile[15]

$$n^2(x, y) = n_0^2 \left(1 - \frac{x^2}{r_x^2} - \frac{y^2}{r_y^2} \right). \quad (1)$$

with n_0 the average refractive index of GaAs and Al_{0.9}Ga_{0.1}As. The eigenfunctions of the associated Helmholtz equation, for the component of the wavefunction transverse to the propagation direction z , are

$$\psi_{[n,m]}(x, y) = H_n \left(\frac{\sqrt{2}x}{w_x} \right) H_m \left(\frac{\sqrt{2}y}{w_y} \right) e^{-\left(\frac{x^2}{w_x^2} + \frac{y^2}{w_y^2} \right)} \quad (2)$$

where H_n and H_m are the Hermite-Gaussian functions of order n and m , respectively. The waist of the fundamental mode is $w_{x,y} = \sqrt{r_{x,y}\lambda_0/(\pi n)}$, where λ_0 is the vacuum wavelength. The eigenvalues associated with the mentioned transverse modes, labeled as $[n, m]$, are the resonance wavelengths of the modes

$$\lambda_{[n,m]} \approx \lambda_{[00]} - n\Delta\lambda_x - m\Delta\lambda_y. \quad (3)$$

. For a quadratic confining potential, the resonance wavelengths of the transverse modes are linearly spaced

$$\frac{\Delta\lambda_{x,y}}{\lambda_0} = \frac{1}{2} \left(\frac{\lambda_0}{n_0\pi w_{x,y}} \right)^2. \quad (4)$$

Gaussian fitting of the intensity profile of the fundamental mode shown in the measurement of Fig.2 yields a spot size of $w_x \approx 2.13 \pm 0.08 \mu\text{m}$ and $w_y \approx 2.25 \pm 0.09 \mu\text{m}$, fully compatible with widths $w_x \approx 2.09 \mu\text{m}$ and $w_y \approx 2.37 \mu\text{m}$ calculated from the transverse mode splitting using Eq.4. From the mode waist one calculate the mode volume $V = (\pi/4)w_x w_y L_{eff}$. The effective cavity length L_{eff} is given by $L_{eff} = L_{cav} + 2L_{pen}$, with $L_{pen} \approx \lambda_0/(4\Delta n)$ (penetration depth into DBR mirrors with index contrast Δn). The Purcell factor can be rewritten as

$$P = \frac{12}{\pi} \mathcal{F} \left(\frac{\Delta\lambda}{\lambda} \right)_{transverse} \quad (5)$$

where ($\mathcal{F} = \lambda_0 Q/(2nL_{eff})$) is the cavity finesse. This relation is important because it gives a quick way to characterize a microcavity, just looking at the spectral separation between the transverse modes. The larger the mode spacing, the smaller the cavity and the larger the Purcell factor.

The quadratic model for $n^2(x, y)$ only works for the lowest-order modes but does not correctly describe correctly the resonance wavelengths of the higher-order modes. This is demonstrated in Fig. 3(a), which shows the measured mode wavelength vs. the theoretical mode wavelength calculated with the parabolic refractive index profile in Eq.1 (for a different cavity than the one on Fig. 2). The experimental mode frequency distribution appears to be super-linear, suggesting that the refractive index profile might be steeper than quadratic. In order to

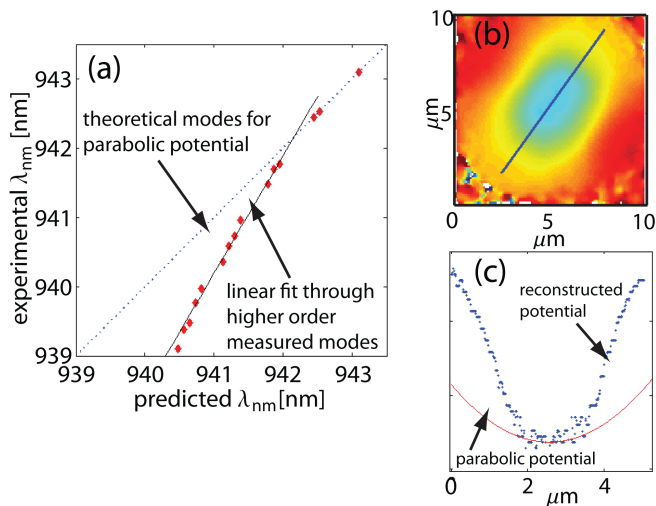


FIG. 3. (a) Super-linear mode frequency distribution of the experimental modes. (b) Reconstruction of the refractive index profile. (c) Refractive index profile cross-section taken from (b). The bottom is fitted to a parabolic potential.

determine the precise refractive index profile, we use the additional information contained in the intensity profiles of the eigenmodes. For this, we write the Helmholtz equation as $\mathcal{H}|\psi\rangle = 0$, where $\mathcal{H} = \partial^2/\partial x^2 + \partial^2/\partial y^2 + V(x, y)$ and $V(x, y) = k_0^2 n^2(x, y)$. Expressing \mathcal{H} in terms of its complete set of eigenvalues ε_n and orthonormal eigenfunctions $|\psi_n\rangle$, we get: $\mathcal{H} = \sum_{n=1}^{\infty} \varepsilon_n |\psi_n\rangle\langle\psi_n|$. In x -representation,

$$V(x) = \langle x | \mathcal{H} | x \rangle = \sum_{n=1}^{\infty} \varepsilon_n |\psi_n(x)|^2. \quad (6)$$

Since only a finite number of modes N can be experimentally measured, we normalized over $\sum_{n=1}^N |\psi_n(x)|^2$. The results, shown in Fig. 3b-c confirm that the refractive index profile is not quadratic, but consists of a flat bottom that corresponds to the un-oxidized region surrounded by steeper walls resulting from the end of the oxidation front.

Until now, we have only considered a scalar theory, justified by the fact that the cavity in Fig. 2 exhibits almost perfect polarization-degeneracy. In general, however, the modes show polarization properties. In particular, the fundamental mode is typically split in two linearly-polarized submodes, with a frequency splitting ranging between 5-50 GHz (compared to a linewidth of about 10 GHz). Such polarization splitting can be ascribed to an asymmetry of the oxidation aperture given by different oxidation rates along different crystal axes [15, 16] or to an intrinsic birefringence of the material (possibly due to strain introduced by the etched trenches[17]). For quantum information applications involving electron spins, the polarization splitting must be removed: techniques to restore perfect degeneracy are reported in the literature [12, 13].

In conclusion, we experimentally characterized spectrally and spatially the confined optical modes of oxide-apertured micropillars. The lower-order modes are well described by Hermite-Gaussian modes, which allows easy mode-matching to external fields, both in free-space and in fibers[18]. We derived a formula to estimate the waist of the fundamental mode and the theoretical maximum Purcell factor from the splitting between the fundamental and the first-order modes. This equation can be used to quickly assess the quality of a device for cavity-QED experiments. Finally, we presented a technique to retrieve the shape of the confining refractive index distribution determined by the oxidation layer, showing that it is flat in the center with steep walls, resulting in a super-linear distribution of the confined modes.

ACKNOWLEDGMENTS

This work was supported by the NSF grant 0901886, the Marie-Curie Award No. EXT-CT-2006-042580, and FOM/NWO Grant No. 09PR2721-2. We thank Nick G. Stoltz for the SEM image in Fig. 1b and Andor for the CCD camera.

-
- [1] S. Strauf, N. G. Stoltz, M. T. Rakher, L. A. Coldren, P. M. Petroff, and D. Bouwmeester, *Nat. Photon.* **1**, 704 (2007).
 - [2] C. Bonato, F. Haupt, S. S. R. Oemrawsingh, J. Gudat, D. Ding, M. P. van Exter, and D. Bouwmeester, *Phys. Rev. Lett.* **104**, 160503 (2010).
 - [3] E. Waks and J. Vuckovic, *Phys. Rev. Lett.* **96**, 153601 (2006).
 - [4] M. T. Rakher, N. G. Stoltz, L. A. Coldren, P. M. Petroff, and D. Bouwmeester, *Phys. Rev. Lett.* **102**, 097403 (2009).
 - [5] S. Reitzenstein, C. Hofmann, A. Gorbunov, M. Strauß, S. H. Kwon, C. Schneider, A. Löffler, S. Höfling, M. Kamp, and A. Forchel, *Applied Physics Letters* **90**, 251109 (2007).
 - [6] S. Reitzenstein and A. Forchel, *Journal of Physics D: Applied Physics* **43**, 033001 (2010).
 - [7] J. P. Reithmaier, G. Sek, A. Löffler, C. Hofmann, S. Kuhn, S. Reitzenstein, L. V. Keldysh, V. D. Kulakovskii, T. L. Reinecke, and A. Forchel, *Nature* **432**, 197 (2004).
 - [8] C. Böckler, S. Reitzenstein, C. Kistner, R. Debusmann, A. Löffler, T. Kida, S. Höfling, A. Forchel, L. Grenouillet, J. Claudon, et al., *Applied Physics Letters* **92**, 091107 (pages 3) (2008).
 - [9] C. Zinoni, B. Alloing, C. Paranthoën, and A. Fiore, *Applied Physics Letters* **85**, 2178 (2004).
 - [10] N. G. Stoltz, M. Rakher, S. Strauf, A. Badolato, D. D. Lofgreen, P. M. Petroff, L. A. Coldren, and D. Bouwmeester, *Appl. Phys. Lett.* **87**, 031105 (2005).

- [11] D. J. P. Ellis, A. J. Bennett, S. J. Dewhurst, P. Atkinson, C. A. Nicoll, D. A. Ritchie, and A. J. Shields, *J. Phys.: Condens. Matter* p. 454212 (2008).
- [12] C. Bonato, D. Ding, J. Gudat, S. Thon, H. Kim, P. M. Petroff, M. P. van Exter, and D. Bouwmeester, *Applied Physics Letters* **95**, 251104 (2009).
- [13] J. Gudat, C. Bonato, E. van Nieuwenburg, S. Thon, H. Kim, P. M. Petroff, M. P. van Exter, and D. Bouwmeester, *Applied Physics Letters* **98**, 121111 (2011).
- [14] G. R. Hadley, *Opt. Lett.* **20**, 1483 (1995).
- [15] E. R. Hegblom, D. I. Babic, B. J. Thibeault, and L. A. Coldren, *Applied Physics Letters* **68**, 1757 (1996).
- [16] R. L. Naone, E. R. Hegblom, B. J. Thibeault, and L. A. Coldren, *Electronics Letters* p. 300 (1997).
- [17] C. Bonato, E. van Nieuwenburg, J. Gudat, S. Thon, H. Kim, M. P. van Exter, and D. Bouwmeester, *Phys. Rev. B* **84**, 075306 (2011).
- [18] F. Haupt, S. S. R. Oemrawsingh, S. M. Thon, H. Kim, D. Kleckner, D. Ding, D. J. Suntrup, III, P. M. Petroff, and D. Bouwmeester, *Applied Physics Letters* **97**, 131113 (2010).